InfraMatics
The Newsletter of Subaudible Sound

NUMBER 21 JUNE 2008

IN THIS ISSUE

IN MEMORY OF HANK BASS

Dear Friends,

As many of you know, our esteemed colleague and friend Hank Bass passed away on May 28, 2008. Hank was a pioneer in many branches of acoustics and director of the National Center for Physical Acoustics at the University of Mississippi, and he took a particular interest in infrasound. Even though each of Hank's many responsibilities vied for his attention, it seemed to us that he devoted much of his time to provide leadership for our growing field and served as a mentor for many of our younger researchers. In late 2002 Hank expressed his concern that our rapidly evolving field needed a place for researchers to publish their work with minimal delay and to learn of new exciting research results by others. He felt we also needed a place to share news in our field. With this idea our online newsletter InfraMatics was born and published its first issue in March, 2003. To date, InfraMatics has released 21 issues containing over 60 research and news articles. This specialized newsletter is but a small part of Hank's legacy.

Hank combined his keen scientific intellect and his considerable influence inside and outside of acoustics to help guide our field towards a bright future. Although Hank moved in rarefied circles in science and politics he never lost his ability to communicate in a very personal and meaningful way with all who knew him. We won't forget his kindness, his friendship and his generosity.

The editorial board of InfraMatics

InfraMatics is an informal series to make available in a timely fashion information about the science of infrasound that any of us might develop. It is provided via our organization's website www.inframatics.org. We expect contributions to InfraMatics to be short and cover only one distinct subject. Figures can be hand-drawn. Lengthy formulae can be stated without derivation. Contributions should be sent to any member of the editorial board by electronic mail. We will assemble all contributions received during a quarter into a single newsletter. The information may be duplicated in the website. We expect that all of us will publish papers that use the material we have previously forwarded to InfraMatics. Everyone is encouraged to do so. To avoid having the material used by someone else in earlier publication, we require that permission to use the material contained in the InfraMatics newsletter by anyone other than the author requires permission by the InfraMatics editorial board. For the time being, Michael Hedlin will act on behalf of the editorial board in such matters.

ATMOSPHERIC ENTRY AND IMPACT OF THE SEPTEMBER 15, 2007 DESAGUADERO METEOROID

K. Antier, A. Le Pichon, Y. Cansi, B. Hernandez, E. Minaya, B. Burgoa, D. Drob, L. G. Evers

ABSTRACT

On September 15, 2007, around 11:45 local time in Peru, near the Bolivian border, the atmospheric entry of a meteoroid produced bright lights in the sky and intense detonations. Soon after, a crater was discovered south of Lake Titicaca. These events have been detected by the Bolivian seismic network and two infrasound arrays operating for the Comprehensive Nuclear-Test-Ban Treaty Organization, situated at about 80 and 1620 km from the crater. The localization and origin time computed with the seismic records are consistent with the reported impact. The entry elevation and azimuthal angles of the trajectory are estimated from the observed signal time sequences and back-azimuths. From the crater diameter and the air-wave amplitudes, the kinetic energy, mass and explosive energy are calculated. The favorable setting of this event provides a unique opportunity to evaluate physical and kinematic parameters of the object which generated the first actual terrestrial meteorite impact seismically recorded.

1. Introduction

The atmospheric entry of meteoroids can generate infrasonic waves often observed at large distances. In most cases, meteoroids sublimate when they penetrate into the upper atmosphere between an altitude of 60 and 100 km. Larger supersonic objects penetrate deeper into the atmosphere and may be modeled as a line source explosion. Although very large objects, like the Tunguska meteoroid, can generate low frequency gravity waves, most of them excite acoustic waves in the infrasound domain (ReVelle, 1997; ReVelle et al., 1998). Such waves are refracted and channeled over long distances by the temperature gradient and the wind structure of the atmosphere (Kulichkov, 1992). Infrasound produced by fragmentations may also be observed a few thousand kilometers away from their origin. At shorter detection distances, the analysis of the recordings presents an opportunity to estimate the entry path, height of thermal bursts, kinetic energy, and other relevant physical characteristics of the meteoroid (Beech et al., 1995; Evers et al., 2001; Brown et al., 2002a; Le Pichon et al., 2002a; ReVelle et al., 2004).

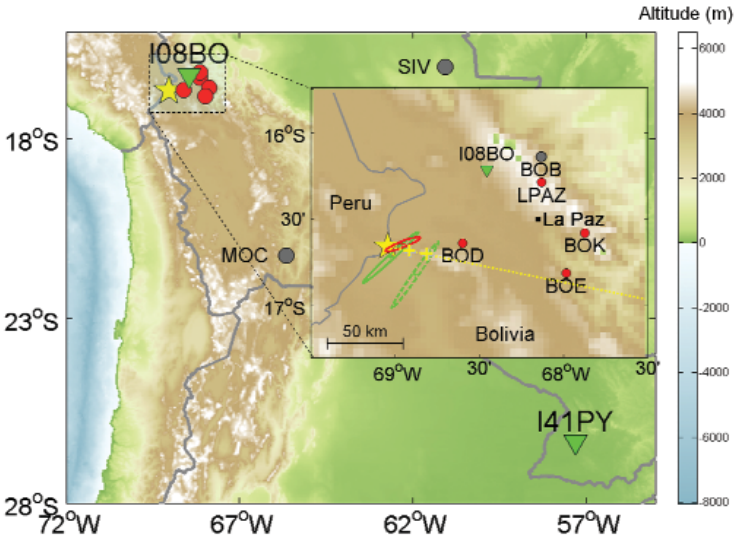

Fig. 1. Location of the Bolivian seismic network and the two I08BO-Bolivia and I41PY-Paraguay infrasound arrays. The yellow star indicates the meteorite impact (16.664°S and 69.044°W, elevation: 3826 m a.s.l.) (Macedo et Macharé, 2007). Red circles indicate stations where signals were clearly detected. At BBOB, MOC and SIV (grey circles), no clear air-waves have been observed. The red 95% confidence ellipse refers to the impact localization using the observed seismic arrivals on BBOD, LPAZ, BBOB, BBOE, BBOK and MOC (Table 2). The green ellipses refer to cross-bearing localizations with the first and second infrasound arrivals detected at I08BO and I41PY (Table 3). The yellow dashed line indicates the trajectory reconstructed from the observed signals (Figure 2). The two yellow crosses indicate possible explosions at altitudes of 21 and 31 km as discussed in Sec. 3.

On September 15, 2007, around 16h40m UTC, inhabitants of Desaguadero, near the border of Peru and Bolivia, reported bright lights in the sky moving in a roughly southwestwards direction (Macedo et al., 2007; Jackson, 2007). A few seconds later, inhabitants of Carancas, in Peru,

heard huge detonations. Damage produced by impacts of ejecta on houses were also reported. Hundreds of meters from this village, a crater was discovered at the coordinates 16.664°S, 69.044°W, and 3826 m altitude. Due to the energy of the impact, mud inside the crater was close to the boiling point. The 13.4 x 13.6 m nearly circular crater was formed in a few meters of soft thick brown saturated sediments from the past ice age stand of Lake Titicaca (Macedo et al., 2007). Close to the crater, material was ejected in two main directions: on the southern side (where the rim is 1 m below the northern one, due to the local topography), and also in the north-northwest direction. At larger distances (100 to 200 m), ejecta was found in all directions (Fig 1). Such a distribution is consistent with the preliminary reported south-westwards trajectory (Jackson, 2007). The water table is about 1.5 m below the surface, and the 5 m-deep crater quickly filled with water, hiding the bottom of the hole and preventing an easy recovery of the main rock fragment remaining from the impact. Fortunately, grey powdering material was found on the rims of the crater, and pieces of the same meteoritic rock were collected tens of meters from it. Their analyses classified it as a H4/5 chondrite type which represents 85% of terrestrial recovered meteorites (Alarcón et al., 2007). Although its size is not exceptional, past studies indicate that a few meteoroids of meter-size collide with the Earth every year (Chyba et al., 1998; Toon et al., 1997; Brown et al., 2002b). The most striking characteristic of this rock is thus not its composition, but the fact that it survived its atmospheric entry without major fragmentation (witnesses reported the fall of a single object), and with enough kinetic energy to create the only chondritic impact crater ever observed in recent times.

Usually, most of the meteoroids entering the terrestrial atmosphere suffer from fragmentation before impacting on the Earth's surface, breaking the rock into smaller fragments that deposit on the surface, barely causing damages, and even rarely creating craters. The first historical reported crater occurred in Eastern Siberia on February 12, 1947, and is associated to the fall of Sikhote-Alin iron meteorite (Krinov, 1971). The initial mass of the meteoroid was estimated to be 100 tons. It fragmented in the Earth's atmosphere into small objects. Altogether 122 impact craters were found with diameters ranging from 0.5 to 26 m and with depths ranging from 1 to 12 m. For some similar events, the trajectory can be partially reconstructed, and meteorites recovered. For example, the Park Forest fireball (March 27, 2004) fragmented three times before reaching the ground (Brown et al., 2004). The Neuschwanstein fireball (April 6, 2002) was also reduced into pieces at the end of its trajectory (Oberst et al., 2004; ReVelle et al., 2004; Spurný et al., 2003), as did the Morávka (May 6, 2000) (Brown et al., 2003), the Tagish Lake (January 18, 2000) (Brown et al., 2002a), and the Peekskill (October 9, 1992) (Beech et al., 1995; Ceplecha et al., 1996) events. Such objects usually produce seismic and acoustic signals when they fragment or when the supersonic front shock sweeps the Earth's surface (Brown et al., 2003).

This event produced seismic and acoustic signals detected by both a regional seismic network and two IMS infrasound arrays. This paper, supported by high quality data, aims to reconstruct the trajectory of the meteoroid and to evaluate some of its physical characteristics. In the first part, a detailed analysis of the seismic and infrasound recordings is carried out. If some signals can be attributed to fragmentation, others are undoubtedly associated with the impact, which is a phenomenon that has never been recorded until now. In the second part, from the observed arrival times of seismic phases, the location and origin time of the impact are calculated with a high degree of certainty. Following the impact localization, the elevation and arrival angles of the bolide are then determined from numerical simulations of infrasonic waves propagating in a realistic atmosphere. In the last part, additional analyses cover source energy estimates from several independent empirical approaches.

2 Observations

The Desaguadero meteoroid entry produced infrasonic waves that have been recorded by two IMS infrasound arrays: I08BO in Bolivia located on the Altiplano and I41PY in Paraguay, 80 km northeast and 1617 km southeast of the crater, respectively (Figure 1). Each of these arrays is composed of four microbarometers, 0.8 to 2.5 km apart. Sensors are MB2000 microbarometers that can measure pressure fluctuations from 0.003 up to 27 Hz. The electronic noise level is 2 mPa rms in the 0.02-4 Hz frequency band over a dynamic range of 134 dB. In order to minimize pressure changes due to surface wind effects, each sensor is connected to an 18-m-diameter spatial noise reducing system (Alcoverro and Le Pichon, 2005). A large meteoroid entry is also likely to produce ground coupled air-waves that can be recorded in seismic stations (Cates and Sturte-

vant, 2001; Arrowsmith et al., 2007). Such seismic signature has been observed on signals recorded by the Bolivian seismic network operated by the Observatory of San Calixto (OSC) in La Paz (Minaya et al., 2007). This network is composed of four vertical short-period stations (BBOB, BBOD, BBOE, BBOK), two three-component short-period stations (LPAZ, MOC), and one three-component short-period and long-period station (SIV). LPAZ and SIV also refer to the primary PS06 and auxiliary AS08 IMS seismic stations, respectively (Figure 1). Table 1 provides the coordinates and locations relative to the crater of the studied seismic and infrasound stations. Five seismic stations, 47 km to 125 km away from the crater, recorded seismic waves from the meteoroid entry and impact.

Figure 2 shows the successive wave trains recorded simultaneously on the two infrasound arrays and the five seismic stations. The first and last detected arrivals (at BBOD and I41PY, respectively) are separated by a nearly 90 minutes time delay (Table 2). The comparable seismic recordings at BBOD, BBOE and BBOK present two clear onsets, while at BBOB and LPAZ, signals are more complex and noisy and do not allow a clear phase identification. The seismic phases marked by the red triangles are consistent with energy originating from the impact location. The difference of few tens of seconds between the observed and the predicted ground coupled air-wave arrival times definitely excludes that these arrivals, as well as the second arrival recorded at I08BO, are associated with the impact.

The wave parameters of the acoustic arrivals measured at I08BO and I41PY are calculated with the Progressive Multi-Channel Correlation (PMCC) method (Cansi, 1995). At I08BO, two transient signals of peak-to-peak am-

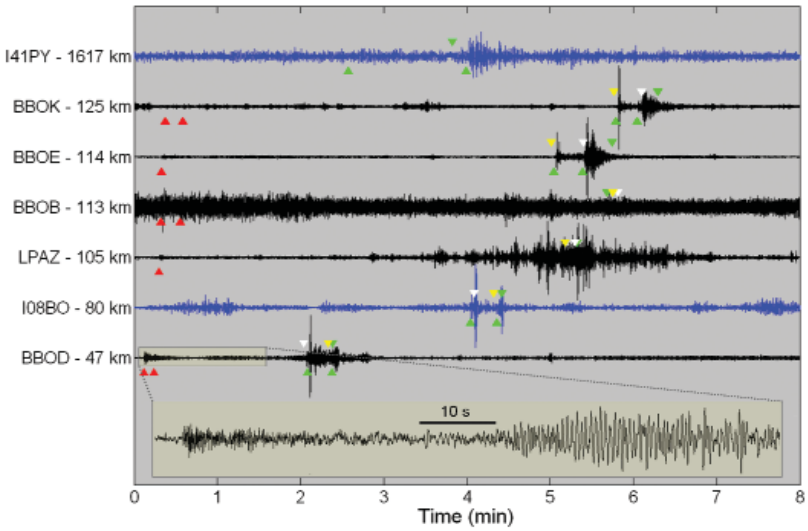

Figure 2. Waveforms (normalized amplitude) at the I08BO and I41PY infrasound arrays (phase aligned traces in blue) band-pass filtered from 1 to 4 Hz, and short-period vertical seismometers part of the Bolivian seismic network (in black). For all recordings, time is relative to the time of impact t0 (16:40:17 UTC), except for I41PY (t0+86 min). At the bottom of the figure, a zoom on the unfiltered recording at BBOD is embedded. This plot indicates a low frequency arrival typical of surface wave from shallow event. The upward-pointing red and green triangles indicate onset times of regional seismic and acoustic waves (infrasound for I08BO and I41BY, and ground coupled air-waves for seismic stations), respectively (Table 2). The downward-pointing green triangles indicate the theoretical arrival times of acoustic waves propagating from the impact location to all receivers with a celerity of 0.33 km/s (with a nearly horizontal propagation), except for I41PY (celerity of 0.30 km/s typical of a stratospheric propagation). The downward-pointing white and yellow triangles refer to the predicted arrival times of acoustic waves generated by two explosions (21 and 31 km above the ground level, respectively) along a trajectory of arrival angle 110° and elevation 50°.

Station	Longitude (°W)	Latitude (°S)	Elevation (m a.s.l.)	Distance (km)	Back-azimuth (°)
BBOD	68.60	16.64	4235	47	266.9
I08BO	68.45	16.21	4131	80	231.7
LPAZ (PS06)	68.13	16.29	4095	105	246.9
BBOB	68.13	16.14	3911	112	239.2
BBOE	67.98	16.81	4325	114	278.4
BBOK	67.87	16.58	4638	125	265.7
MOC	65.64	21.25	621	621	324.2
SIV (AS08)	61.07	15.99	849	854	263.9
I41PY	57.31	26.34	164	1617	309.1

Table 1: Name, coordinates, distance from the crater and true back-azimuth of the short-period vertical seismic sensors (LPAZ, BBOB, BBOE, BBOK, MOC and SIV) and the two IMS infrasound arrays (I08BO-Bolivia and I41PY-Paraguay) that provided data.

Station	Pg	Sg	I1	I2
BBOD	16:40:23.5	16:40:30.9	16:42:22	16:42:41
I08BO			16:44:10	16:44:34
LPAZ	16:40:35.4			unclear
BBOB	16:40:35.8	16:40:49.9		noisy
BBOE	16:40:36.3		16:45:21	16:45:41
BBOK	16:40:39.2	16:40:52.0	16:46:05	16:46:21
I41PY			18:08:51	18:10:10

Table 2: Observed arrival times of regional seismic waves, ground coupled air-waves on seismic sensors (sampling rate of 50 Hz) and infrasonic waves at I08BO and I41PY (sampling rate of 20 Hz). Arrivals I1 and I2 do not necessarily originate from the same part of the trajectory of the meteoroid.

plitude 1.7 and 1.2 Pa, are detected with values of horizontal trace velocity (0.345 km/s) slightly greater than the sound speed at the ground level (0.333 km/s), which indicates a wave propagation with a ~15° shallow elevation angle. The back-azimuth of the first arrival is compatible with acoustic waves originating from the impact. Conversely, even taking into account propagation effects and uncertainties in wave parameter calculations, the back-azimuth of the second arrival (~15° larger than the expected bearing) can not be associated to it. Simple geometrical considerations regarding the path of the bolide relative to the location of I08BO suggest that shock waves or thermal bursts can explain the second arrival if the arrival azimuth of the trajectory (clockwise from North) is greater than 53° (Sec. 3.2). At I41PY, 1617 km away from the crater, two signals of much weaker amplitude (10 and 20 mPa) are detected. Both arrival times and back-azimuths are consistent with energy propagating in the stratospheric duct (Sec. 3.3). Table 3 summarizes the main characteristics of the detected coherent wave trains at I08BO and I41PY.

3 Propagation modeling and trajectory

3.1 TRAJECTORY RECONSTRUCTION

Because fluctuations in the sound speed are generally much smaller than wind variations in the upper atmosphere, it is important to account for wind conditions in order to match the predicted arrivals with the observed signals. Wind and temperature profiles used in our simulations are provided by the European Centre for Medium-Range Weather Forecasts model (ECMWF, http://www.ecmwf.int) from the ground to about 85 km altitude, and the MSISE-90 and HWM-93 empirical reference models (Hedin 1991; Hedin et al., 1996) for higher altitudes. At the time of the event and in the vicinity of the source region, the wind profiles exhibit a rich vertical structure. Due to the increase of the effective sound speed profile (sound speed corrected for the horizontal wind terms in the direction of propagation), stratospheric returns are expected for an azimuth ranging from 70 to 270°.

The impact source location is calculated from the Pn and Sn waves refracted at the Moho, and the Pg and Sg direct crustal waves at stations BBOB, BBOD, BBOE, BBOK and LPAZ (Table 2). A local seismic magnitude of 1.45 is derived from the seismic recordings. The clear low frequency wavetrain is observed on the closest station to the impact (BBOD) (Figure 2), which is typical of shallow seismic events propagating in water-saturated soils. The back-azimuth of 246.3° calculated from the LPAZ three-component short-period station is consistent with energy originating from the crater. Using a standard non-linear least square inversion procedure (Coleman and Li, 1996) and a two-layer regional velocity model, the following co-

Station	Arrival time (UTC)	Back azimuth (°)	Trace velocity (km/s)	Celerity (km/s)	Peak-peak amplitude (Pa)	Dominant frequency (Hz)
I08BO	16:44:10	227.4	0.345	-	1.70	1.7
	16:44:34	214.6	0.344	-	0.86	1.2
I41PY	18:08:51	309.0	0.354	0.305	0.02	1.1
	18:10:10	308.5	0.352	0.3	0.04	1.6

Table 3. Main characteristics of the detected coherent acoustic waves at I08BO and I41PY. With a sampling rate of 20 Hz, the expected numerical resolution at 1 Hz is of the order of 0.5° for the azimuth and 5 m/s for the horizontal trace velocity.

ordinates and impact time are derived: 16.64°S - 68.96°W, 8 km away from crater, at 16:40:16.7 UTC. Cross-bearing localizations associating the first and second infrasound arrivals detected at I08BO and I41PY are also indicated on Figure 1 (16.72°S - 69.02°W at 16:40:07, and 16.85°S - 68.89°W at 16:40:55, 7 and 26 km east of the crater, respectively). These two localizations account for uncertainties in the azimuth estimates due to transversal wind effects on the propagation (~5°). The observed coordinates of the crater (16.66°S - 69.04°W) and the impact origin time derived from the seismic localization (16:40:16.7 UTC) are considered here as ground truths. From this location, different set of possible trajectories are explored by minimizing residuals between the observed and predicted arrival times of ground coupled air-waves.

The entry speed of a meteoroid has an upper limit. The Earth orbits the Sun at a mean speed of 30 km/s in a heliocentric referential in the apex direction, and the speed of a meteoroid with an elliptic orbit in the Solar system can not exceed 42 km/s (Solar system escape velocity). Thus, the speed relative to the Earth can range from 0 km/s (from the antapex direction with a 30 km/s speed) to 72 km/s (frontal collision with the Earth). According to the time and location of the impact, the relative speed of the Desaguadero meteoroid can range from 0 km/s to 57 km/s. The Earth escape velocity of 11.7 km/s defines the minimum initial speed of any meteoroidal object entering the atmosphere. This velocity is nearly constant when the object penetrates the first upper layers of the atmosphere. Below 30 km altitude, the meteoroid generally slows down as the altitude decreases (ReVelle et al., 2004). In a first approximation, we assume that the entry speed of the studied event is 20 km/s above 30 km, and below, linearly decreases with the altitude down to 1 km/s. Due to the contrast between the meteoroid supersonic speed and the sound speed, the infrasound measurements alone could not yield more precise values for the entry velocity. The travel time of the infrasonic waves mainly depends on the vertical structure of the wind and temperature profiles. Consequently, the solutions found using different initial and final supersonic speeds of the meteoroid always range within the uncertainty bounds indicated below.

With such a speed model, the rectilinear trajectory is only defined by its elevation and azimuthal angles. On the basis of the existing visual reports, the elevation (relative to the horizontal) and azimuthal angles (clockwise from North) range from 10 to 80° and -50 to 170°, respectively. We focus on the two clear arrivals observed at stations I08BO, BBOD, BBOE and BBOK, which are likely related to the same origin. In order to explain the observed time sequences of acoustic arrivals, ray paths and travel times are computed using the Tau-P ray tracing code (Garcés et al., 1998) for each point of the trajectory using the atmospheric conditions.

At supersonic speeds, pressure waves combine and form a Mach cone radiating away from the generation point (ReVelle, 1976). At several tens of kilometers from the bolide, signals do not exhibit the typical N-wave signature, but rather appear in the form of the observed pulses (Pierce and Maglieri, 1972). We first assume that the detected air-waves propagated in a direction normal to the Mach cone whose opening angle β is given by $\sin(\beta) = Cz/Vz$, where Cz and Vz, are respectively the sound and meteoroid speeds at the altitude z. In our simulations, rays are launched at different angles determined both by the speed and trajectory of the bolide, and the ECMWF sound speed profile. The source is thus approximated by a linear distribution of elementary Mach cones. Waves normal to the Mach cones are defined by unique azimuthal and elevation angles (Le Pichon et al., 2002b). For stations I08BO, BBOD, BBOE and BBOK (I41PY, ~1600 km away from the source, is discarded due to large uncertainties in travel time calculations), the minimum time residual is found to be less than 5 s for a east-westards (azimuth = 100+/-30°) trajectory with a 40+/-3° elevation angle (Figure 3A). However, the results do not predict more than one arrival at all stations. Furthermore, such source model can not explain the infrasound arrivals at I41PY station, as the front wave propagates nearly perpendicularly to the trajectory of the fireball. Finally, the large azimuth residuals (greater than 50°) indicate that this trajectory is far from being the most plausible.

We also make the simplifying assumption that the detected signals were generated by two main thermal blasts radiating isotropically. The minimum time residual is then found for two fragmentations occurring at altitudes of 21+/-2 km and 31+/-2 km above the ground level, along a trajectory of azimuth 110+/-20° and elevation 50+/-10° (Figures 2 and 3B). Figure 2 compares the observed arrival times to the predicted ones. This approach explains both the arrival times of the two onsets detected at I08BO, BBOD, BBOE and BBOK with a mean residual of 5 s, as well as the de-

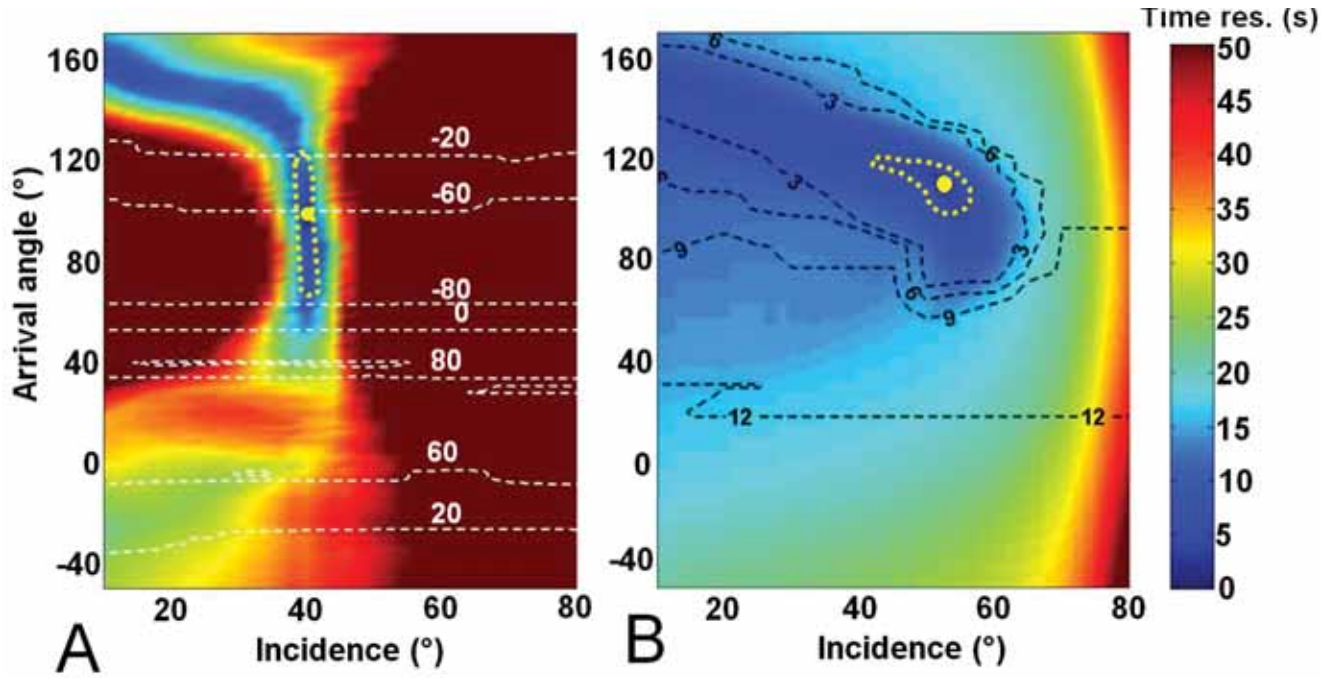

Figure 3. Time (colormap) and back-azimuth (contour lines) residuals calculated for different sets of trajectories. A trajectory is defined by its arrival and incident angles. For each set of arrival and incidence angles, rays are launched for 100 points along the trajectory. The mean arrival time residuals (in seconds) account for the two arrivals detected at BBOB, BBOK, BBOE and I08BO. The arrival time and back-azimuth residuals are calculated using two different models: (A) propagation normal to the Mach cone, (B) point-like sources mimicking the two fragmentations. The yellow dots indicate the minimum of the arrival time residuals. The yellow contour lines outline the area where residuals are lower than 5 s. The back-azimuth residuals (in degrees) are calculated for the points along the trajectories that minimize the time residuals.

tected back-azimuths at I08BO with a maximum error of 2° (Figure 3B). The time difference between signals at BBOE and BBOK corroborate this path (Figure 2). At a horizontal distance of 70-75 km from the fragmentations, simulations predict shallow elevation angles for rays reaching I08BO, with celerity values consistent with the observed ones.

3.2 LONG RANGE PROPAGATION

Infrasound propagation is significantly affected by the vertical and horizontal wind structure where wind-induced refraction can trap or disperse sound energy. Advances in parabolic equation methods recently provided a new tool for studying atmospheric infrasound propagation at local and regional scales using enhanced atmospheric specifications. In order to gain additional physical insight into the observed signals at I41PY, simulations are carried out using a wide angle and high Mach number parabolic equation for sources radiated isotropically located at different altitudes (Lingevitch et al., 2002). The Naval Research Laboratory Ground-to-Space (NRL-G2S) model (Drob et al., 2003) includes recent atmospheric data sets, improved parameterization of the atmospheric vertical structure, and capabilities for near-real time global assimilation of tropospheric and stratospheric winds. In order to get accurate simulation results, the NRL-G2S model was run to provide a self-consistent atmospheric specification (sound velocity and wind speed profiles) for September 15, 2007 at 16:00 UTC, over a grid of 0.5 x 0.5 degree, from ground level to 150 km altitude, with a vertical resolution is 0.25 km. Figure 4 presents the simulation results for a source altitudes ranging from 10 to 50 km at a frequency of 1 Hz. As expected, thermospheric returns are strongly attenuated and are not measurable over such long range. A dominant elevated stratospheric waveguide is observed between 10 and 35 km. A small fraction of the stratospheric energy bounces the Earth's surface and reaches the infrasound array. Assuming a point-like source model, the signal attenuation is larger than 70 dB for a source altitude below 10 km and above 50 km. The source altitude should thus range between 10 and 50 km where a much weaker attenuation is predicted (~40 dB).

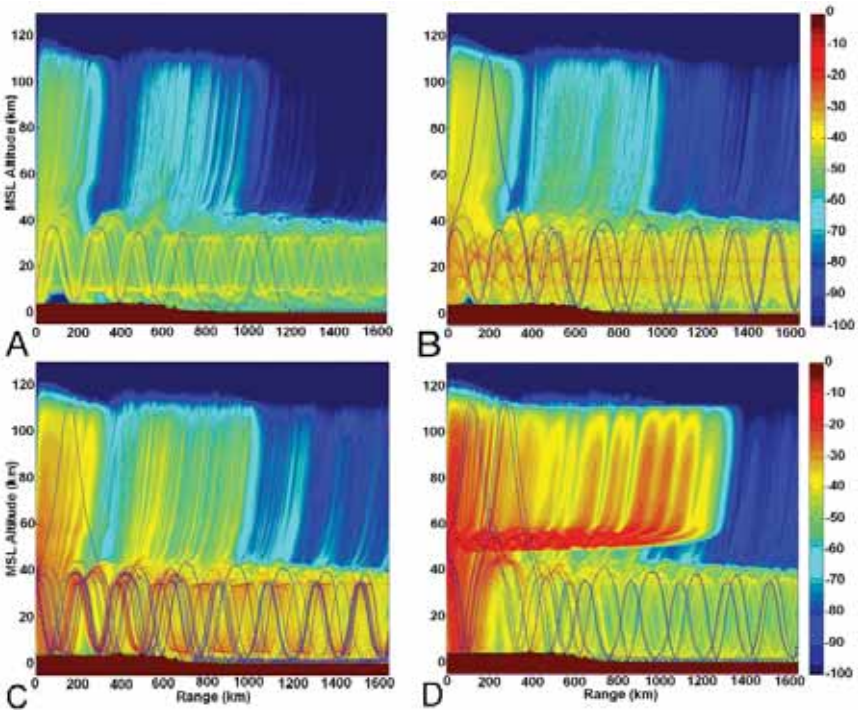

Figure 4. Propagation of infrasonic waves in the direction of I41PY for different source heights (A, B, C, D: 10, 25, 35 and 50 km, respectively) and a frequency of 1 Hz. The NRL-RAMPE parabolic equation method (Lingevitch et al., 2002) combined with the environmental profiles derived from the G2S atmospheric model are compared to a 3D ray traces adapted from the Tau-P method (Garcés et al., 1998). Since effects of the boundary conditions of the propagation domain are particularly important in the high-altitude Andes region, simulations account for the NOAA Global Land One-km Base Elevation (GLOBE) digital terrain elevation model (Hastings and Dunbar, 1998). According to these simulations, the recorded signals at I41PY can be explained by multiple stratospheric returns.

For these arrivals, ray tracing predicts back-azimuth corrections lower than 2° due to the transverse wind component which slightly deflects the rays from the original launch direction. At 20 km altitude, the predicted celerity values for the two signals (0.295 to 0.305 km/s) are consistent with the predicted ones (0.305 and 0.300 km/s). The observed horizontal trace velocities (0.354 and 0.352 km/s, Table 3), are also consistent with the simulated ones. Such celerity and trace velocity values are typical of a stratospheric propagation (Brown et al., 2002). According to these simulations, the two coherent wave trains at I41PY can either be interpreted as two consecutive stratospheric returns or be associated with the two fragmentations discussed above.

4 Size and energy estimation

Using a drastic simplification, a massive body penetrating the atmosphere, with a velocity considerably greater than the speed of sound, instantaneously looses a large part of its kinetic energy during ablation process (Ceplecha and ReVelle, 2005). It suffers such a strong deceleration that it is fragmented before reaching the ground surface. The explosive energy released by the two fragmentations is calculated by applying semi-empirical relations based on the infrasonic recordings at I08BO and I41PY. The most striking effect of the sudden release of the remaining kinetic energy is the formation of the crater. From the observed crater diameter and the total ejected volume, the equivalent explosive energy released by the impact, the mass and diameter of the impactor are evaluated.

4.1 EXPLOSIVE ENERGY

As used by Evers and Haak (2001), the explosive energy released by fragmentation can be calculated by applying the following semi-empirical relation based on infrasonic recordings from low altitude nuclear explosions (Whitaker and ReVelle, 1995; ReVelle, 1997):

$$\log_{10}(E_s/2) = 3.34 \log_{10}\left(\frac{1}{f_{obs}}\right) - 2.58 \qquad (1)$$

where f_{obs} is the dominant frequency at the maximum amplitude (in Hz) and E_s represents the energy (in kilotons of a TNT equivalent explosion) limited to $E_s < 100$ kt. Using the above relation, with the measured frequency listed in Table 3, the yield of the fragmentation ranges from 0.9 to 2.9 tons (I08BO), and from 1.1 to 3.8 tons TNT (I41PY).

An important parameter for event characterization is also the amplitude. Actually, atmospheric winds strongly affect the recorded signals. Edwards et al. (2006) examined the correlation between infrasonic amplitude and yield, and derived the following expression:

$$W = 10^{3(a-kVs)/b}\, R^3\, A^{-3/b} \qquad (2)$$

where R is the source to receiver range (in km), A is the maximum peak-to-peak amplitude (in Pa), V_s is the ve-

locity of the stratospheric wind in the source-receiver direction (in m/s), and *(a, b, k)* are empirical constants (Mutschlecner and Whitaker, 1990). Edwards et al. (2006) had to distinguish between small and large bolides to find their regression fits. Assuming that the energy released by each fragmentation is lower than 7 kt (which is highly probable according to the previous calculations), the constants are: a = 3.36+/-0.60, b = -1.74+/-0.24 and k = -0.0177 s/m. At a distance of 1617 km, I41PY recorded stratospheric arrivals of amplitude 0.02 and 0.04 Pa (Table 3). Using these values and a constant effective stratospheric wind of 30 m/s, a yield of 1.0 to 3.2 tons TNT is found. These yield estimates derived from two independent empirical approaches are here in good agreement.

4.2 METEOROID DIAMETER

Holsapple (1993) reviewed the scaling laws for impact processes and related the mass and velocity of the impactor to the crater size and type of soil. In the strength regime, the strength of the soil is large compared to the lithostatic pressure, thus the latter can be ignored. This assumption is valid for meter-sized objects. For a crater in wet soil in the strength regime, Holsapple (1993) derived:

$$L \propto 0.05\, m\, V^{1.65} \qquad (3)$$

where L is the crater volume (in m^3), m is mass of the impactor (in kg) and V its speed (in km/s). With a depth of 5 m and a diameter of 13.5 m, a total ejected volume of 480 m^3 (half-volume of an ellipsoid) is estimated. For an impact speed ranging from 0.8 to 3 km/s), the mass of the meteoroid ranges between 1.5 and 15 tons. With a chondritic density of 3.5, a corresponding meteoroid diameter between 1 and 2 m is calculated. Since only objects of diameter greater than one meter are able to touch down (Brown et al., 1996), such values are acceptable.

\4.3 ENERGY RELEASED BY THE IMPACT AND SPEED ESTIMATES

The yield of an explosion can be determined based on the crater size. Glasstone (1957) used crater sizes of nuclear tests of yield W, in the range of 1 to 20,000 kT TNT, and derived that the diameter scales with $W^{1/3}$, and the depth with $W^{1/4}$. Kinney and Graham (1985) used 200 large surface explosions and found that the crater diameter d scales with the explosive yield W in kg TNT as:

$$d = 0.8\, W^{1/3} \qquad (4)$$

Using the above relation and the reported crater diameter, the yield is determined as 4.8 tons. It is noteworthy that in this case, the crater is caused by a moving object impacting on the Earth's surface rather than an explosive point source.

Considering that during the impact, in addition to thermal losses, a fraction of the kinetic energy is transmitted through the soil and the atmosphere, a speed lower limit of the impactor can be estimated from the kinetic energy E_k formula,

$$E_k = \frac{1}{2}\, \tilde{n}\, \left(\frac{\partial d^3}{6} \right) V^2 \qquad (5)$$

where ρ is the density (in kg/m^3), d is the diameter of the meteoroid (in m), and V is the speed (in m/s). According to this relation, the lowest terminal speed is 1.5 km/s, which is consistent with the speed model defined in Sec. 3.2.

From the time of occurrence of the two fragmentations, the estimated trajectory, the air-waves arrival times at stations BBOD, BBOE, and BBOK, and the predicted Tau-P travel times, a maximum speed of 10 km/s is evaluated below 27 km altitude. In the first upper layers of the atmosphere above 30 km, the speed of the meteoroid is nearly constant (ReVelle et al., 2004). Therefore, with an entry speed of 11.7 km/s, a meteoroid diameter of 2-4 m before ablation and a chondritic density of 3.5, the initial energy released would range from 1 to 8 kt TNT equivalent. More observations would certainly reduce the upper limit source energy, yielding a more realistic estimate of the initial kinetic energy.

5 Concluding remarks

The terrestrial impact of the Desaguadero meteoroid near the Bolivia's border with Peru has been detected by the Bolivian seismic network at a range of 125 km. At a distance of 1617 km from the crater, along the dominant stratospheric wind direction, infrasonic waves are associated with the entry of the meteoroid. Ray tracing simulations based on a supersonic moving point source, consider both shock waves generated by an almost cylindrical line emission and acoustic emission from point-like explosions. The conclusion of this analysis is that fragmentations were probably the dominant processes in the production of sound during the entry, rather than the hypersonic shock of the meteoroid passage through the atmosphere. Mean residuals between the predicted and observed arrival times indicate that the strongest infrasonic

signals probably originated from two main thermal bursts at altitudes of 25 and 35 km above sea level, along a trajectory of azimuthal angle 110° and elevation 50°. The back-azimuths and elevation angles of the two coherent wave trains detected at I08BO are consistent with the location and time of occurrence of these fragmentations. This path corroborates the apparent trajectory reported at the town of Desaguadero. Moreover, a recent and independent study by Brown et al. (2008) yields similar results derived from different set of data.

On the basis of the recorded signals at I08BO and I41PY, consistent yield estimates of the fragmentations are derived from independent empirical approaches. The explosive energy released by the two fragmentations is evaluated between 1.0 and 3.8 t TNT equivalent. From the crater diameter and the total ejected volume, a rock of 1 to 2 m-diameter would have released an explosive energy of 4.8 tons TNT. The detailed analysis of the seismic and infrasound recordings suggests a rather low initial entry speed of the meteoroid (~12 km/s) which may explain why it survived its atmospheric entry without major fragmentation before impacting the Earth. Further studies gathering additional measurements, such as visual observations, could reduce uncertainties in our estimates, and would thus help in evaluating more realistic ranges of the physical and kinematic parameters of this.

According to the existing statistics and observations, such an event is to happen every few years (Chyba et al., 1998; Toon et al., 1997; Brown et al., 2002b). This work applies to a natural event various technical and analytical detection methods developed with the aim of monitoring the CTBT. It demonstrates the value of seismo-acoustic synergy to obtain precise location of a naturally occurring source. With the increasing number of IMS and regional cluster of seismo-acoustic networks deployed around the globe, along with a continuation of research in the field of infrasound monitoring, meteor entry evidences would probably occur more frequently in the next years. It is also expected that the development of enhanced near real-time atmospheric specifications and new numerical simulation capabilities will improve our knowledge of meteor characteristics.

Acknowledgements

The authors are grateful to Dr. L. Jackson (Geophysical Survey of Canada), Dr P. Brown (Western University of Ontario), Dr. Gonzalo Tancredi (Institute of Physics of Montevideo, Uruguay), M. Davis (North American Meteor Network), Drs. J.M. Guerin, S. Legarrec and J. Vergoz (CEA), and N. Brachet (CTBT-O) for their interest in this study, helpful discussions and improvements of the manuscript. We thank J.P. Santoire and P. Herry (CEA) for their expertise in analyzing seismic and infrasound data. We also thank the NASA Goddard Space Flight Center, Global Modeling and Assimilation Office (GSFC-GMAO), and the NOAA National Centers for Environmental Prediction (NCEP) for providing the NWP data that went into the NRL-G2S atmospheric specifications.

References

Alarcón H. B., and E. Gorinova 2007. Estudio Microscopico del Meteorito de Huanu Collo. Instituto de Investigaciones Geológicas y del Medio Ambiente - Carrera « Fisica ». Fac. De Ciencias Puras–UMSA Planetario Max Schreier, 8 pages, fcpn.umsa.bo/fcpn/app?service=external/Planetarium_AreaView&sp=241.

Alcoverro B., and A. Le Pichon 2005. Design and optimization of a noise reduction system for infrasonic measurements using elements with low acoustic impedance. *J. Acoust. Soc. Am.*, 117, doi:10.1121/1.1804966.

Arrowsmith, S. J., D. P. Drob, M. A. H. Hedlin, and W. Edwards 2007. A joint seismic and acoustic study of the Washington State bolide: Observations and modeling, *J. Geophys. Res.*, 112, D09304, doi:10.1029/2006JD008001.

Bass H. E., and L. C. Sutherland 2004. Atmospheric absorption in the atmosphere up to 160 km. *J. Acoust. Soc. Am.*, 115, 1012-1032.

Beech M., P. Brown, R.L. Hawkes, Z. Ceplecha, K. Mossman, and G. Wetherhill 1995. The Fall of the Peekskill Meteorite: Video observations, atmospheric path, fragmentation record and orbit. *Earth, Moon, and Planets,* 68, 189-197.

Brown P., A. R. Hildebrand, D. Green, D. Page, C. Jacobs, D. O. ReVelle, E. Tagliaferri, J. Wacker, and B. Wetmiller 1996. The fall of the St-Robert meteorite. *Meteorit. Planet. Sci.,* 31, 502-517.

Brown P., D. O. ReVelle, E. Tagliaferri, and A.R. Hildebrand 2002a. An entry model for the Tagish Lake fireball using seismic, satellite and infrasound records. *Meteorit. Planet. Sci.,* 37, 661-675.

Brown P., R. E. Spalding, D. O. ReVelle, E. Tagliaferri, and S. P. Worden 2002b. The flux of small near-Earth objects colliding with the Earth. *Nature,* 420, 294-296.

Brown P., P. Kalenda, D. O. ReVelle, and J. Borovička 2003. The Morávka meteorite fall: 2. Interpretation of infrasonic and seismic data. *Meteorit. Planet. Sci.,* 38, 989-1003.

Brown P., D. Pack, W. N. Edwards, D. O. ReVelle, B. B. Yoo, R. E. Spalding, and E. Tagliaferri 2004. The orbit, atmospheric dynamics, and initial mass of the Park Forest meteorite. *Meteorit.*

Planet. Sci., 39, 1781-1796.

Brown P., D.O. ReVelle, E.A. Sukara, W.N. Edwards, S. Arrowsmith, L.E. Jackson, G. Tancredi, D. Eaton 2008. Analysis of a crater forming meteorite impact in Peru. *J. Geophys. Res.,* in press.

Cansi Y. 1995. An automatic seismic event processing for detection and location: the PMCC method. *Geophys. Res. Lett.,* 22, 1021-1024.

Cates J. E., and B. Sturtevant 2002. Seismic detection of sonic booms. *J. Acoust. Soc. Am.,* 111, No.1, Pt. 2, 614-628.

Ceplecha Z., P. Brown, R. L. Hawkes, G. Wetherill, M. Beech, and K. Mossman 1996. Video observations, atmospheric path, orbit and fragmentation record of the fall of the Peekskill meteorite. *Earth, Moon, and Planets,* 72, 395-404.

Ceplecha Z., and D. O. ReVelle 2005. Fragmentation model of meteoroid motion, mass loss, and radiation in the atmosphere. *Meteorit. Planet. Sci.,* 40, 35-54.

Chyba C. F., G. E. Van Der Vink, and C. B. Hennet 1998. Monitoring the Comprehensive Test Ban Treaty: Possible ambiguities due to meteorite impacts. *Geophys. Res. Lett.,* 25, 191-194.

Coleman T. F., and Y. Li 1996. An Interior, trust region approach for nonlinear minimization subject to bounds. *SIAM J. on Optimization,* 6, 418-445.

Drob D., J. M. Picone, and M. Garcés 2003. The global morphology of infrasound propagation. *J. Geophys. Res.,* 108, doi:10.1029/2002JD003307.

Drummond J. D. 1981. A test of comet and meteor shower associations, *Icarus,* 45, 545-553.

Edwards W. N, P. G. Brown, and D. O. ReVelle 2006. Estimates of meteoroid kinetic energies from observations of infrasonic airwaves. *J. Atmosph. and Solar-Terrestrial Phys.,* 68, 1146-1160.

Evers L. G., and H. W. Haak 2001. Listening to sounds from an exploding meteor and oceanic waves. *Geophys. Res. Lett.,* 2, 41-44.

Garcés M., R. A. Hansen, and K. G. Lindquist 1998. Travel times for infrasonic waves propagating in a stratified atmosphere. *Geophys. J. Int.,* 135, 255-263.

Glasstone S. 1957. The effect of nuclear weapons, U.S. Atomic Energy Commission, Washington, D.C. 196-227.

Hastings D. A., and P. K. Dunbar 1998. Development and assessment of the Global Land One-km Base Elevation Digital Elevation Model (GLOBE). International Society of Photogrammetry and Remote Sensing, Archives, 32, 218-221.

Hedin A. E. 1991. Extension of the MSIS thermosphere model into the middle and lower atmosphere. *J. Geophys. Res.,* 96, 1159-1172.

Hedin A. E., E. L. Fleming, A. H. Manson, F. J. Schmidlin, S. K. Avery, R. R. Clark, S. J. Franke, G. J. Fraser, T. Tsuda, F. Vial, and R. A. Vincent 1996. Empirical wind model for the upper, middle and lower atmosphere. *J. Atmos. and Terrestrial Phys.,* 58, 1421-1447.

Holsapple K. A. 1993. The scaling of impact processes in planetary sciences. *Ann. Rev. of Earth and Planetary Sci.,* 21, 333-373.

Jackson L. J. R. 2007. Personal communication, Geological Survey of Canada.

Kinney G. F., and K. J. Graham 1985. Explosive shocks in air, Springer-Verlag, New York. 9-10.

Krinov E. L. 1971. New studies of the Sikhote-Alin iron meteorite shower. *Meteoritics,* 6, 127-138.

Kulichkov S. N. 1992. Long-range propagation of sound in the atmosphere: A review *Izvestiia Russian Academy of Sciences, Atmosheric Oceanic Physics,* 28, n°4, pp.339-360.

Le Pichon A., J. M. Guérin, E. Blanc, and D. Raymond 2002a. Trail in the atmosphere of the December 29, 2000 meteorite as recorded in Tahiti: characteristics and trajectory reconstitution. *J. Geophys. Res.,* 107, doi:1029/2001JD001283.

Le Pichon A., M. Garcés, E. Blanc, M. Barthélémy, and D.P. Drob 2002b. Acoustic propagation and atmosphere characteristics derived from infrasonic waves generated by the Concorde. *J. Acoust. Soc. Am.,* 111, 629-641.

Lingevitch J. F., C. Michael, D. Dalcio, D. Douglas, R. Joel, and S. William 2002. A wide angle and high Mach number parabolic equation. *J. Acoust. Soc. Am.,* 111, doi:10.1121/ 1.1430683, 729-734.

Macedo L. F., and J. O. Macharé 2007. The Carancas meteorite fall, 15 Sept. 2007. Official INGEMMET initial report, 5 pages.

Minaya E, P. Rougon, D. Valero, G. Fernandez, E. Lazaro, and W. Cano 2007. The Bolivian Seismic Network. *Eos Trans. AGU,* 88, Jt. Assem. Suppl., Abstract S34A-02.

Mutschlecner J. P., and R. W. Whitaker 1990. The correction of infrasound signals for upper atmospheric winds. NASA, *Proc. 4th Int. Symp. on Long-Range Sound Propagation,* 143-153.

Oberst J., D. Heilein, U. Köhler, and P. Spurný 2004. The multiple meteorite fall of Neuschwanstein: Circumstances of the event and meteorite search campaigns. *Meteorit. Planet. Sci.,* 39, 1627-1641.

Pierce A. D., and D. J. Maglieri 1972. Effects of atmospheric irregularities on sonic-boom propagation. *J. Acoust. Soc. Am.,,* 51, 702-720.

ReVelle D. O. 1976. On meteor-generated infrasound. *J. Geophys. Res.,* 81, 1217-1230.

ReVelle D. O. 1997. Historical detection of atmospheric impacts of large super-bolides using acoustic-gravity waves. *Annals of the New York Academy of Sciences,* 822, 284-302.

ReVelle D. O., R. W. Whitaker, and W.T. Armstrong 1998. In-

frasound from the El Paso Super-bolide of October 9 1997. *SPIE Conference on Characteristics and Consequences of Space Debris and Near-Earth Objects,* San Diego, California.

ReVelle D. O., P. G. Brown, and P. Spurný 2004. Entry dynamics and acoustics/infrasonic/seismic analysis for the Neuschwanstein meteorite fall. *Meteorit. Planet. Sci.,* 39, 1605-1626.

Southwork R. B., and G. S. Hawkins 1963. Statistics of meteor streams. *Smithsonian Contributions to Astrophysics,* 7, 261-285.

Spurný P., J. Oberst, and D. Heinlein 2003. Photographic observations of Neuschwanstein, a second meteorite from the orbit of the Příbram chondrite. *Nature,* 423, 151-153.

Toon O. B., R. P. Turco, and C. Covey 1997. Environmental perturbations caused by the impacts of asteroids and comets. Annals of the *New York Academy of Sciences,* 822 , 401–402.

Whitaker R. W., and D. O. ReVelle 1995. Analysis of the acoustic conversion efficiency for infrasound from atmospheric entry of NEO's. Los Alamos National Laboratory, *LA-UR-95-4121.*

Contact the Authors

K. Antier, A. Le Pichon, Y. Cansi, and B. Hernandez
Commissariat à l'Energie Atomique, Centre DAM - Ile de France, Département Analyse Surveillance Environnement, Bruyères-le-Châtel, 91297 Arpajon Cedex, France

E. Minaya and B. Burgoa
Observatorio San Calixto, Calle Indaburo 944 - Casilla 12656, La Paz, Bolivia

D. Drob
E. O. Hulbert Center for Space Research, Naval Research Laboratory, 4555 Overlook Ave, Washington, DC 20375, USA

L. G. Evers:
Royal Netherlands Meteorological Institute, Seismology Division, PO Box 201, 3730 AE De Bilt, Netherlands

ANNOUNCING A SPECIAL SESSION AT THE 2008 AGU FALL MEETING

Dear Colleagues,

Please consider a contribution to the following session at the upcoming 2008 AGU Fall Meeting, in San Francisco.

V26: OBSERVATIONS AND MODELING OF VOLCANIC BLASTS AND JETS

Description: Explosive volcanic degassing consists of a combination of discrete blasts and more continuous jet flows, depending on the gas volume and overpressure. Well-developed turbulent jet flows can either transition with altitude into thermally buoyant plumes, or collapse to form pyroclastic flows. This type of volcanic activity is amenable to direct observation by visual, thermal, radar, infrasonic, and seismic instrumentation. Numerical and analogue models, as well as analyses of pyroclastic deposits, provide further insight into the fluid dynamics of these processes. This session integrates observations and numerical and analogue modeling of volcanic blasts and jets. We encourage contributions that show observations or models that can provide constraints on jet flow structure, mass fluxes, vent overpressures, jet dimensions and velocities, the influence of vent and crater geometry, temperature or composition of ejecta, and ballistic velocities.

Index Terms: 8428 8414 8445 8419 8404.

The abstract submission deadline is 10 September 2008, 2359 UT. Full submission guidelines can be found at: www.agu.org/meetings/fm08

Robin Matoza, David Fee, and Milton Garces

Contact the Authors

Robin Matoza
Laboratory for Atmospheric Acoustics, University of California, San Diego, rmatoza@ucsd.edu

David Fee
Infrasound Laboratory, University of Hawaii, dfee@isla.hawaii.edu

Milton Garces
Infrasound Laboratory, University of Hawaii, milton@isla.hawaii.edu